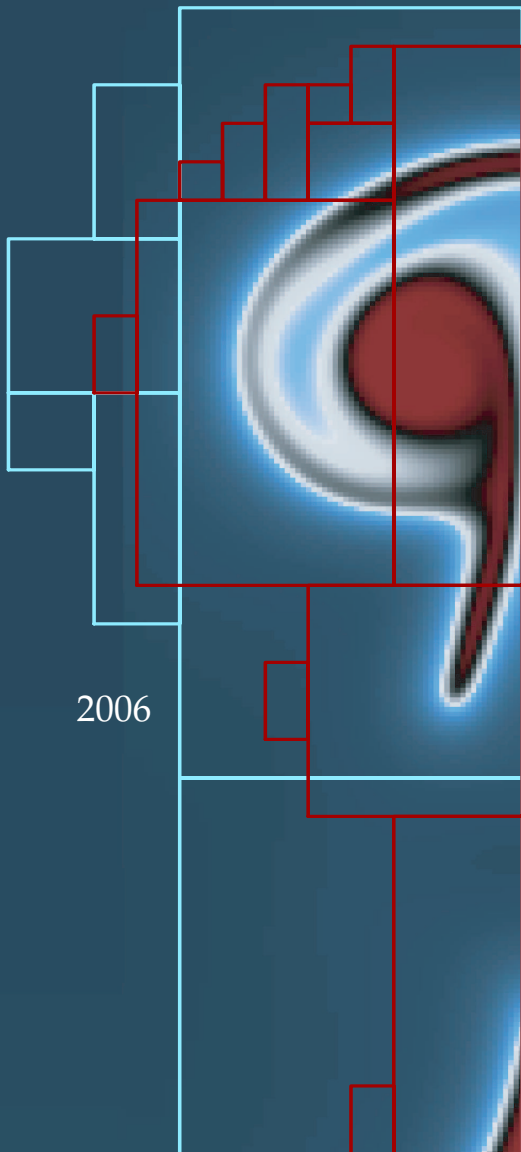


*Communications in
Applied
Mathematics and
Computational
Science*

Volume 1

No. 1

2006



**NONLOCAL DAMAGE ACCUMULATION AND FLUID FLOW IN
DIATOMITES**

GRIGORY ISAAKOVICH BARENBLATT,
MICHIEL BERTSCH AND CARLO NITSCH



mathematical sciences publishers

NONLOCAL DAMAGE ACCUMULATION AND FLUID FLOW IN DIATOMITES

GRIGORY ISAAKOVICH BARENBLATT,
MICHIEL BERTSCH AND CARLO NITSCH

We investigate a new model for fluid flows in diatomite formations recently introduced by Barenblatt, Patzek, Prostokishin and Silin. We provide numerical evidences of the existence of a sharp front between the damaged and the undamaged rock, and we study the structure of this front. Finally, we simulate some infield operations and we set up a qualitative model control problem to maximize the profit during the oil extraction.

1. Introduction

In the last decades oil-bearing diatomite formations have attracted special attention. An example of this kind of deposits is the giant oil fields of Lost Hills and Belridge in California. The development of such deposits has some characteristic properties due to certain peculiarities of diatomaceous rocks: high porosity, very low permeability in the pristine state, and fragility. Because of the high porosity, the diatomite oil reservoirs are often very rich, but, in view of the low permeability, the wells placed in this kind of oil reservoirs have very low productivity unless the hydraulic fracture technique is applied. This technique, which basically consists of injection under high pressure of very viscous fluid from the wells inside the reservoir, increases rock permeability. However, because of fragility, a long-term fracturing process causes subsidence phenomena, with very serious consequences for the safety of the wells themselves. Therefore, though the damaging process is necessary to increase production, it has to be monitored to avoid well collapse.

Recently a new model of fluid flows through diatomaceous rocks was introduced by Barenblatt, Patzek, Prostokishin and Silin [2], taking into account the microstructural changes in diatomites that occur during the filtration of fracturing fluid. In [Section 2](#) we shall review its physical background. The model contains several functional relationships and coefficients which cannot be chosen quantitatively

MSC2000: primary 76S05; secondary 74A45, 35K65.

Keywords: flow in porous media, oil engineering, continuum damage mechanics, degenerate parabolic system.

without further experimental study. In this paper we restrict ourselves to power-type functional relationships. In this case, the model leads to the system

$$\begin{cases} \partial_t \omega = \left[\Lambda^2 \nabla(\omega^\mu (p - I)_+^\beta \nabla \omega) + A(1 - \omega)(p - I)_+^\gamma \right]_+, \\ \partial_t p = K \nabla(\omega^\alpha \nabla p), \end{cases}$$

where the subscript “+” indicates the positive part. The equations are obtained by averaging over the height of the diatomaceous stratum, and thus the problem becomes two-dimensional; the pressure of the fluid at a point \mathbf{x} and time t is denoted by $p(\mathbf{x}, t)$, and, as usual in continuum damage mechanics, $\omega(\mathbf{x}, t)$ is the so-called “damage parameter”, with values between 0 and 1. The constant I takes into account the strength of the rock; μ is a nonnegative constant and Λ , K , α , β , γ , and A are positive constants.

As can be easily observed from the second equation, we have made the assumption that in the undamaged rocks, where $\omega = 0$, the permeability vanishes. Already in [2] it was conjectured that this assumption leads to a free boundary problem. In other words, we expect that there exists an *a priori* unknown front that separates the damaged and undamaged rocks. A justification of this assumption is supplied by experimental observations (see the satellite photograph in Figure 1). Throughout this paper we shall show numerical simulations which validate such a conjecture,

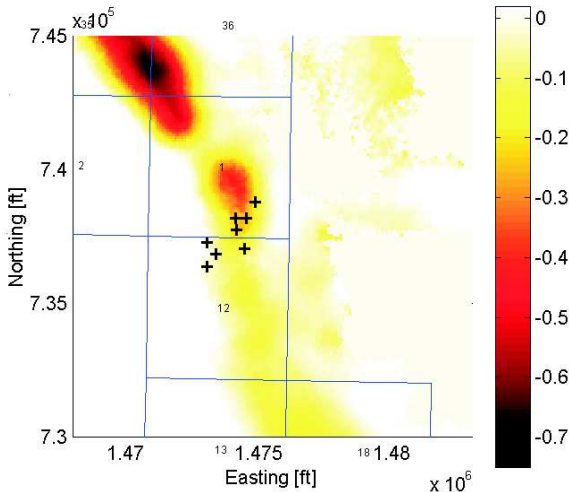


Figure 1. The wells that failed in South Belridge diatomaceous deposit in the year 2000 were located outside the large subsidence bowl. Surface subsidence in mm/day. Courtesy of T. W. Patzek, D. B. Silin (UC Berkeley, LBNL) and E. J. Fielding (NASA JPL).

and for a slightly simplified form of the system it is even possible to perform an analytical investigation (see [5; 4]) which leads to the same conclusion.

This model of fluid flow in diatomites has a wide range of applications, and in this paper we show some of them by simulating infield operations. We simulate several wells placed in five points formation and compute the accumulation of damage and the fluid extraction rate. Moreover we shall set up some model control problems for which it makes sense to look for an optimal strategy, if we impose some feasible restriction on the fluid pressure variations at the wells.

2. Physical background

We remind that the model we shall consider has been specifically introduced in order to deal with the filtration of fluids in a very special kind of rocks called diatomites. A typical picture of the microstructure of the diatomite as it is observed with an electronic microscope is given in [Figure 2](#). The peculiarities of the diatomite in its pristine state are: a very large bulk porosity m that can be up to 70%, and a very low permeability k , of the order of 0.1–1 md (10^{-12} – 10^{-11} cm²) and even less; therefore, for practical purposes, in its pristine state it can be considered as impermeable. For this reason some of the wells in the Lost Hills field in California at the beginning of the primary recovery had a very low, practically zero, production. In fact, the oil production in diatomaceous deposits started only when the technique of hydraulic fracturing was applied.

Hydraulic fracturing, a technology developed in the 1950s, gave producers the possibility to extract more oil out of newly discovered and existing fields. Powerful pumps at the surface inject a fluid (in the beginning a viscous fluid carrying sand was

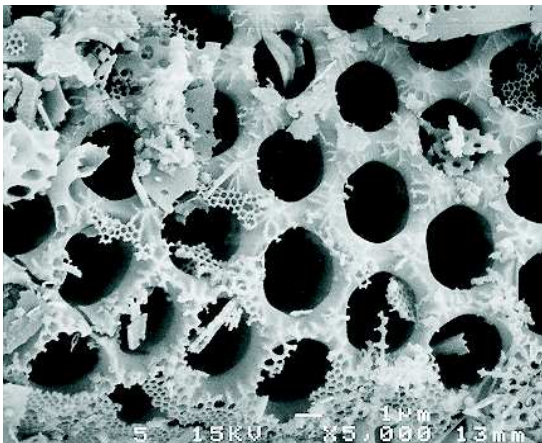


Figure 2. The fragile microstructure of the diatomite rock in SEM microphotograph. Courtesy of Prof. T. W. Patzek.

used, the so-called “fracture fluid”) into the reservoir rocks. The pressure exerted by the fluid exceeds the compressive stress of the rock, opening fractures which constitute paths of increased permeability. Thus, when the pressure is released, the sand supports the crack opening and the fluid can flow more easily. Sometimes injection and extraction are performed through the same well.

In diatomaceous oil-bearing formations like Lost Hills, hydraulic fracturing is performed by injecting water. Owing to the peculiarities of the diatomite, the microstructure of this rock has to change to get any appreciable fluid flow. Actually, during field operations the stress in the rock leads to the collapse of wall pores, resulting in a network of microcracks that increases the permeability of the diatomite. Eventually, the microcrack net connects with the macrofracture. Such an interaction of fractures at different scales, which goes down to the microscopic level, is a peculiarity of the diatomite oil-bearing formations, and motivated the development of a new model based on the continuum damage mechanics approach.

We start from the assumption that the filtration of the fluid and the accumulation of cracks are strongly coupled, so that we have to derive a model which solves simultaneously the macroscopic fluid flow and the microstructural changes of diatomite.

We begin from the filtration equation of the fluid in the diatomaceous stratum. We make the following simplifying assumptions:

- A1. *Water and oil are not distinguished.* Thereafter we use the word “fluid” to refer to both species.
- A2. *The diatomaceous stratum is homogeneous, with constant height and depth, and bounded from above and below by impermeable rocks.*
- A3. *Inside the reservoir, during geologic times, the pressure p of the fluid and the mean geostatic stress σ assumed, respectively, the constant values p_i and σ_i .* (The mean geostatic stress is $\frac{1}{3}(\sigma_x + \sigma_y + \sigma_z)$, that is, one-third of the first invariant of the stress tensor.)
- A4. *The deposit is “deep”.* This assumption together with A3 implies that also if we perturb the fluid pressure p from its equilibrium initial value p_i , the sum $p + \sigma$ remains constant and is equal to $p_i + \sigma_i$ during the whole process.
- A5. *The diatomite is a weakly compressible elastic porous medium.*
- A6. *The fluid is weakly compressible, so its density ρ is a linear function of pressure.*

Under such hypotheses, following [2] (see also [1]), we obtain from the continuity equation $\partial_t(m\rho) + \nabla(\rho\mathbf{u}) = 0$ (where \mathbf{u} is the filtration velocity) and from Darcy’s law $\mathbf{u} = -(k/\mu)\nabla p$ (where μ is the fluid viscosity) the equation for the pressure:

$$\partial_t p = \nabla(\mathcal{K}\nabla p). \quad (1)$$

Here the “piezo-diffusivity” coefficient \mathcal{K} is defined as

$$\mathcal{K} = \frac{k}{\mu mc},$$

where c is a constant taking into account the compressibility coefficient of the fluid and the compressibility coefficient of the rock porosity. Equation (1) is defined in two spatial dimensions, and all the quantities involved (pressure, porosity, permeability, compressibility, etc.) have to be interpreted as averaged over the height of the diatomaceous stratum.

The key idea in [2] was to consider permeability no longer as a fixed quantity, but as a function of the rock damage, $k = k(\omega)$. In subterranean mechanics sometimes one uses pressure-dependent permeability, but we will neglect this dependence. We will also neglect the contribution to the porosity, given by the microcracks opened during the damage accumulation, because the volume fraction of cracks is small.

The basic equation now becomes

$$\partial_t p = \nabla(\mathcal{K}(\omega) \nabla p). \quad (2)$$

Here $\mathcal{K}(\omega)$ is a fast growing function of ω , and $\mathcal{K}(0) = 0$ by hypothesis. In [2] no further assumption was made about the form of $\mathcal{K}(\cdot)$ due to the lack of experimental evidence. However, in the following, in order to perform a numerical and analytical investigation, we will assume as a first step that $\mathcal{K}(\omega) = K\omega^\alpha$, $\alpha > 0$. Clearly, the permeability is the function of time and space, but here we assume that the space and time variability of permeability is due only to space and time variability of damage.

To complete the problem formulation, it is now necessary to add an equation for the damage accumulation. Initially the rock is considered pristine ($\omega = 0$), with the possible exception of small regions around the wells that appear during the drilling. When the water is pumped into the wells and starts to filtrate in the diatomaceous rock, the pressure in the pores eventually increases above a certain critical value I and microcracks start to appear. The exact value of I is unknown and has to be determined by infield experiments. We claim that it has to be not less than p_i , since during geological time no damage has been accumulated (we neglect seismic and tectonic effects).

It is natural to make the basic assumption that locally the damage accumulation rate $\partial_t \omega$ is proportional to a certain power of $(p - I)_+$, and also proportional to the fraction of undamaged bonds $1 - \omega$. Therefore, as in classical continuum damage mechanics, the process of damage accumulation is governed locally by a kinetic equation of the following type:

$$\frac{d\omega}{dt} = A(1 - \omega)(p - I)_+^\gamma,$$

where A is a constant. In addition, together with this bulk mechanism, we also consider a nonlocal damage diffusion process. We expect, in fact, that fluid wedging take place in the microcracks. Again, we are focused on qualitative evaluation of the equations, and we choose a very simple nonlocal damage evolution equation, in the form

$$\partial_t \omega = [\nabla(D(\omega, p) \nabla \omega) + A(1 - \omega)(p - I)_+^\gamma]_+, \quad (3)$$

where the positive part on the right hand side avoids a nonphysical damage healing. In particular, we will use the expression

$$D(\omega, p) = \Lambda^2 \omega^\mu (p - I)_+^\beta$$

for the damage diffusivity coefficient, where Λ is constant.

3. The mathematical problem formulation

Equations (2) and (3) are the starting point for a mathematical formulation of the problem of fluid flow in diatomaceous rocks, leading to the following nonlocal damage accumulation and pressure evolution model:

$$\begin{cases} \partial_t \omega = [\Lambda^2 \nabla(\omega^\mu (p - I)_+^\beta \nabla \omega) + A(1 - \omega)(p - I)_+^\gamma]_+, \\ \partial_t p = K \nabla(\omega^\alpha \nabla p), \end{cases} \quad (4a)$$

$$\omega(\mathbf{x}, 0) = \omega_0(\mathbf{x}), \quad (4b)$$

$$p(\mathbf{x}, 0) = p_0(\mathbf{x}), \quad (4c)$$

where $\omega_0(\mathbf{x})$ and $p_0(\mathbf{x})$ are given initial distributions of the damage and pressure. We will refer to system (4) as the *2D formulation of the “diatomite problem”*.

We remind that ω is the vertically averaged damage in the oil-bearing layer of diatomite rock, while p represents the averaged pressure of fluid contained in the stratum. Moreover, I is related to the strength of the material and represents a threshold pressure under which no damage accumulation or diffusion occurs. In the *analytical* investigation, we assume for simplicity that $p = 0$ corresponds to the rest pressure of the fluid, p_i , in the undamaged zone. Therefore we shall also assume $I \geq 0$. The constants $\alpha, \beta, \gamma, \mu$ and A satisfy

$$\alpha, \beta, \gamma, A > 0 \quad \text{and} \quad \mu \geq 0. \quad (5)$$

System (4) exhibits two major mathematical difficulties:

- the nonnegativity of $\partial_t \omega$, which physically represents the condition of no healing but which mathematically renders the equation for ω “fully nonlinear”;
- the degeneracy of the diffusion coefficients $\omega^\mu (p - I)_+^\beta$ and ω^α if $\omega = 0$ and $p \leq I$.

We also consider the one-dimensional version of Equation (4a)

$$\begin{cases} \partial_t \omega = \left[\Lambda^2 \partial_x (\omega^\mu (p - I)_+^\beta \partial_x \omega) + A(1 - \omega)(p - I)_+^\gamma \right]_+ \\ \partial_t p = K \partial_x (\omega^\alpha \partial_x p). \end{cases} \quad (6)$$

We will refer to it as the *1D formulation of the diatomite problem*. In spite of its simplification, such a formulation is traditional. Let us consider for example a huge number of wells placed along a straight line and operating simultaneously: this is customary for oil and water filtration problems, see the book [1] as well as the comprehensive book [3]. Therefore it might be useful to replace a discrete representation of the wells by a homogeneous distribution density of wells along the line. This representation is called *drainage gallery*, and it works quite fine as soon as we are not too close to the wells. The 1D formulation can very likely describe the case where a drainage gallery is orthogonal to the x axis.

4. Numerical examples for the two-dimensional formulation

In this section we investigate some numerical examples for the 2D formulation of the diatomite problem (4). Just to understand what happens in a very simple case, we present a first example in which a single well placed in the center of an ideal squared oil field injects fluid at constant pressure. This will help to capture the qualitative behavior of the pressure and damage evolution inside the diatomite stratum.

Subsequently, we simulate an oil field composed by five wells placed in diamond formation (five points scheme). In this formation four of them are located in the corners of a square and one is placed in the center of this square. This formation is frequently used in oil fields, where usually the wells placed in the corners are injectors, and the one in the center is a production well. We will simulate this situation, but we will also do the opposite, using the corner wells as production ones and the central one as injection well. For numerical simulations, we idealize the oil field as a square with vertices $(\pm L, \pm L)$. The wells are represented by circles of radius $L/10$. In the diamond formation, four of them are centered in $(\pm 0.4 \cdot L, \pm 0.4 \cdot L)$, the fifth is centered in the origin. For the computation we first rewrite the problem (4) in a nondimensional form. The spatial variables (x, y) are replaced by nondimensional ones: $(\eta, \zeta) \equiv (L^{-1}x, L^{-1}y)$. In the new coordinates, the gradient is $\tilde{\nabla} \equiv L\nabla$. We use the nondimensional pressure $P \equiv p/\tilde{p}$, where \tilde{p} is a certain constant with the dimension of pressure. Finally, we define the

nondimensional time $\theta = t \Lambda^2 \tilde{p}^\beta L^{-2}$. If we choose \tilde{p} such that $\tilde{p}^\beta = K/\Lambda^2$, we get

$$\begin{cases} \partial_\theta \omega = \left[\tilde{\nabla}(\omega^\mu (P - \mathbb{1})_+^\beta \tilde{\nabla} \omega) + \tilde{a} (1 - \omega) (P - \mathbb{1})_+^\gamma \right]_+, \\ \partial_\theta P = \tilde{\nabla}(\omega^\alpha \tilde{\nabla} P) \end{cases}, \quad (7)$$

Here, $\mathbb{1} = \frac{I}{\tilde{p}}$ and $\tilde{a} = \frac{A \tilde{p}^{\gamma-\beta} L^2}{\Lambda^2}$.

The pressure is initially everywhere equal to a constant $P_0 < \mathbb{1}$. When an injection well starts working, the pressure inside the corresponding circle is raised to a value $P_{\max} > \mathbb{1}$. In these examples the values of parameters are: $P_0 = 2$, $P_{\max} = 10$, $P_{\min} = 0$ and $\mathbb{1} = 5$.

In the circle corresponding to a production well, the pressure is lowered to a value $P_{\min} < P_0$. The initial damage is prescribed to be equal to 0 in the whole domain, except in the wells where it is equal to 1. We have chosen for these examples $\alpha = 2$, $\gamma = 5$, $\beta = \tilde{a} = 1$, $\mu = 0$, and we prescribed no flux boundary conditions on the sides of the square. Finally, we have discretized the side of the domain in 161 points, and in order to handle the nonlinearity and the degeneracy we have used an implicit finite difference scheme.

Example 4.1. The first example represents a single injection well placed in the center of a squared region. The idea is to demonstrate the sharp front that separates damaged and undamaged regions and that coincides with the pressure front. We remind to the reader that the formation of the sharp front separating perturbed and unperturbed regions is a well known feature for degenerate parabolic equations such as ‘‘porous medium equations’’ (see [1] and references therein). In the following, it will be clear that the degeneracies involved in system (7) make the problem much more complicated than standard ones. The simulation runs from $\theta = 0$ to $\theta = 0.6$. At time $\theta = 0$ the well starts working and the damaged region coincides with the one occupied by the well. Figure 3 shows pictures corresponding to $\theta = 0.09$ and $\theta = 0.6$.

Example 4.2. In this second example a production well is placed in the center of a square, while the injection wells are in the corners. The configuration is schematically represented in Figure 4.

The simulation runs from $\theta = 0$ to $\theta = 0.21$. At time $\theta = 0$, the injection wells start working, while the production well initially is at rest and starts working at time $\theta = 0.15$. The reason for this delay is that we wait until the damaging zone propagating from the injection wells reaches the production well. The results are represented in Figures 5–8. Figure 7 (bottom) shows the vector field of the velocity of the fluid inside the oilfield at $\theta = 0.21$. Figure 8 shows on the same graph the flux of fluid injected and extracted.

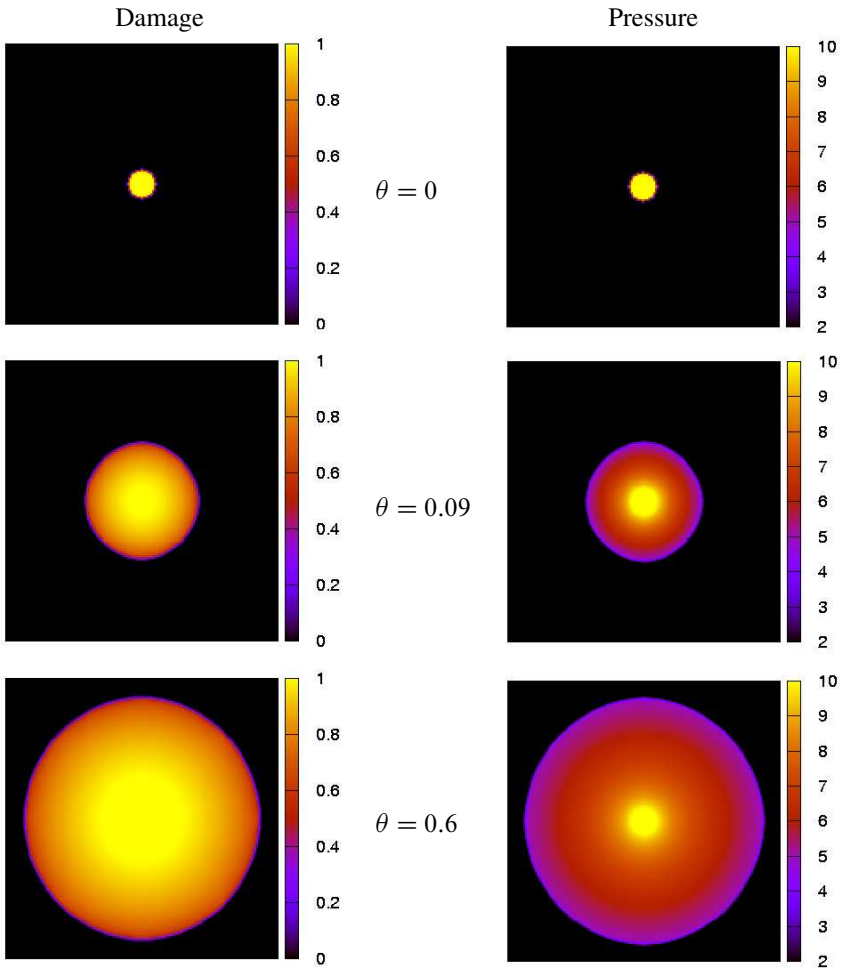


Figure 3. Extension of damage and pressure with increasing time θ .

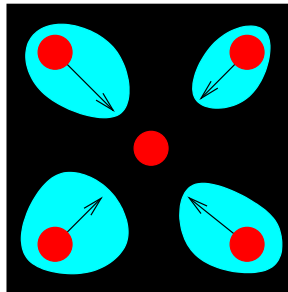


Figure 4. Schematic configuration of wells in the oil field. The center spot indicates the production well, the rest injection wells.

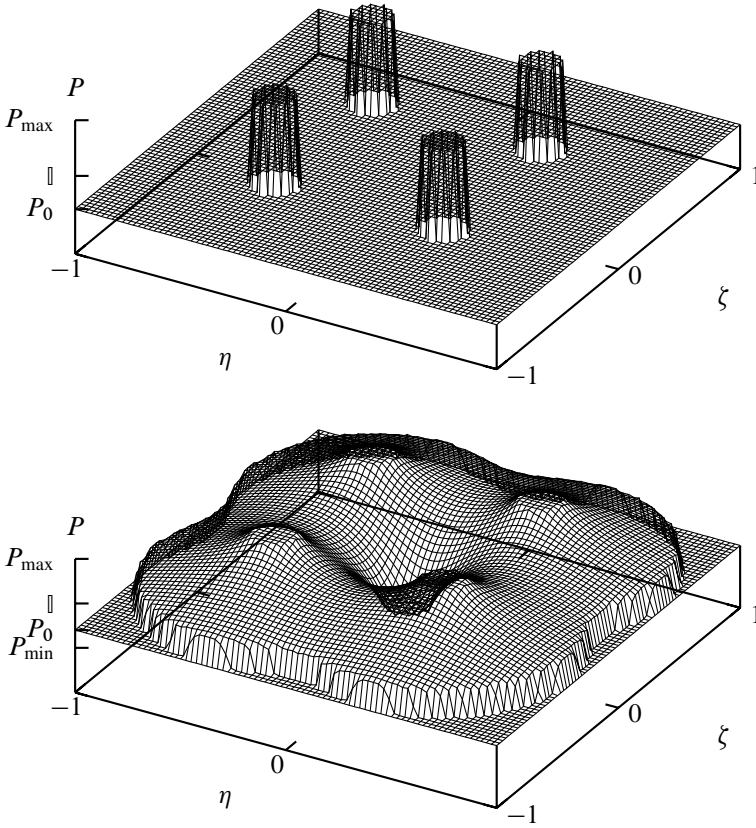


Figure 5. Initial pressure (top) and pressure at $\theta = 0.21$ (bottom). All the wells are active.

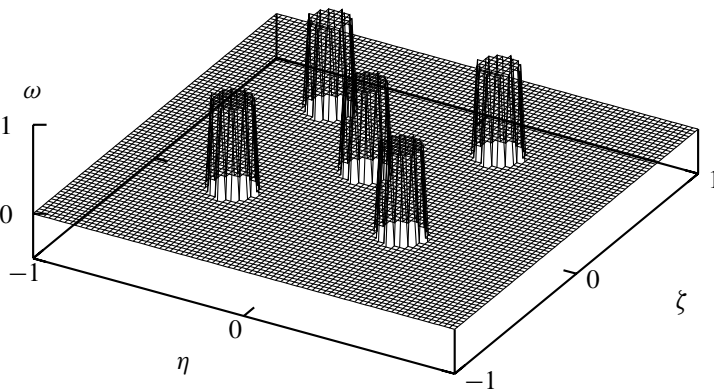


Figure 6. The initial damage ($\theta = 0$) is concentrated around the five wells.

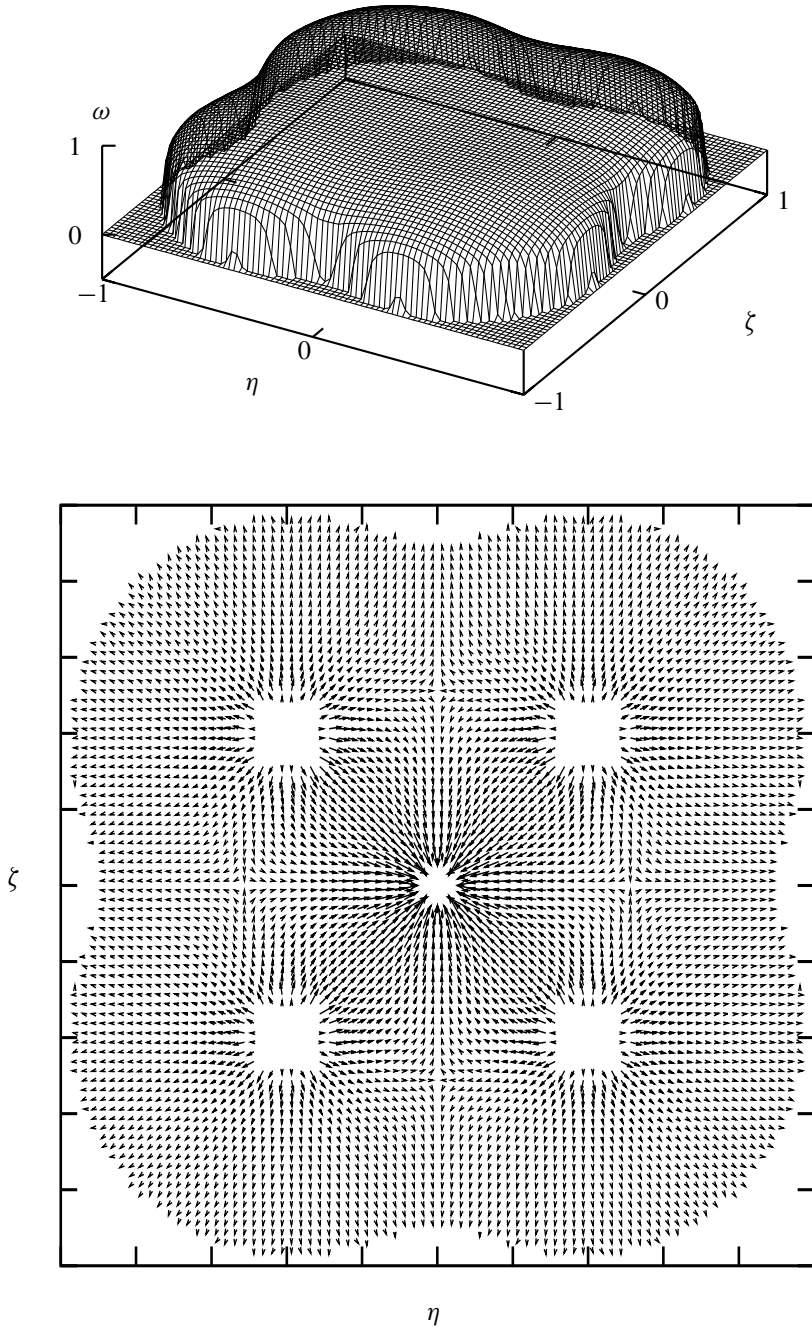


Figure 7. Damage (top) and fluid velocity field (bottom) at $\theta = 0.21$.

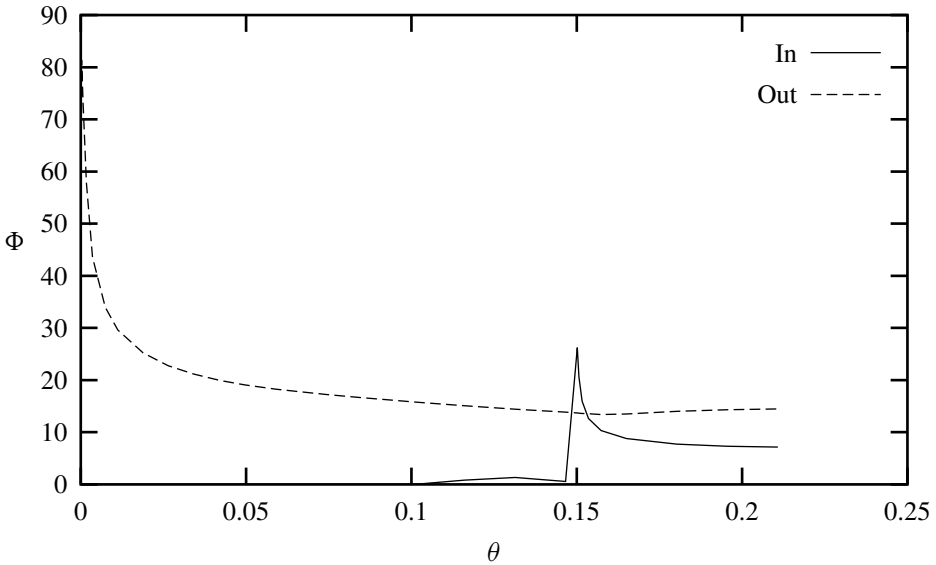


Figure 8. The total amount of fluid recovered per unit of time (Out), and the total amount of fluid injected per unit of time (In), are plotted as functions of the nondimensional time θ . At $\theta \approx 0.1$ the damage front reaches the production well. At $\theta = 0.15$ the production well starts working.

Example 4.3. In this example, the well placed in the middle is an injection well, while those placed in the corners are production wells. The configuration is schematically represented in [Figure 9](#).

The simulation runs from $\theta = 0$ to $\theta = 0.56$. At time $\theta = 0$, only the injection well is working, while the production wells start working at $\theta = 0.2$. The results

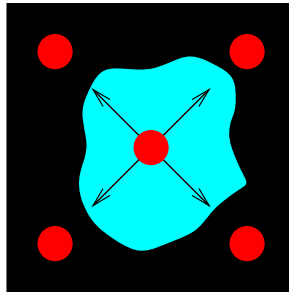


Figure 9. The schematic configuration of the wells in the oil field. The spot in the center corresponds to the injection well. The spots in the corners are the production wells.

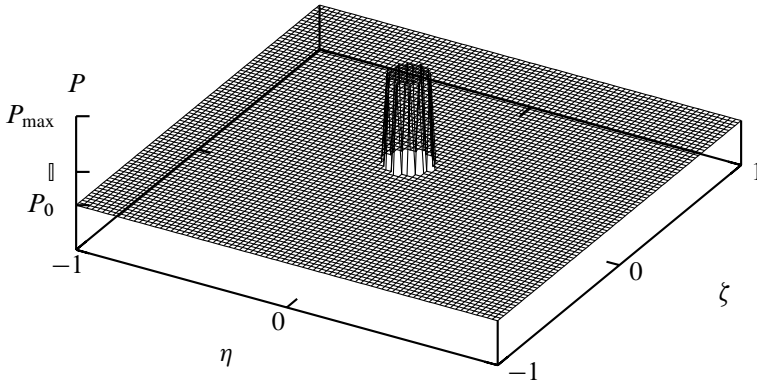


Figure 10. The initial pressure. Only the central well is active, and injecting water.

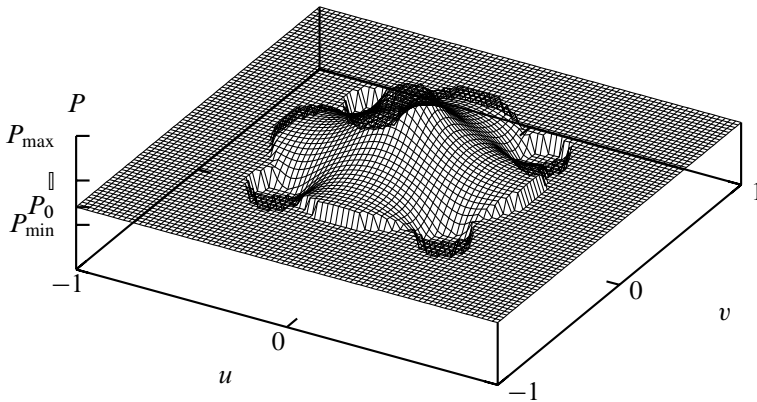


Figure 11. The pressure at $\theta = 0.56$ when all the wells are active.

are presented in Figures 10 through 13. In Figure 12 (bottom) we notice that the flux line starting from the injection well reaches the production wells. Actually, Figure 13 clearly shows that after a certain transition time the injected fluid flux is equal to the extracted fluid flux.

These simple examples are the first step of a numerical investigation of the 2D model. First of all, the numerical simulations confirm the conjecture that there is a sharp front between the damaged and undamaged zones. We emphasize again (see [1]) that such sharp fronts are a common feature of the degenerate parabolic equations of the type considered in the present work. In addition, in Example 4.3 we observe the main consequence of the threshold constant I . As expected, the front propagation stops when the pressure at the front goes below the value \mathbb{I} ; see Figure

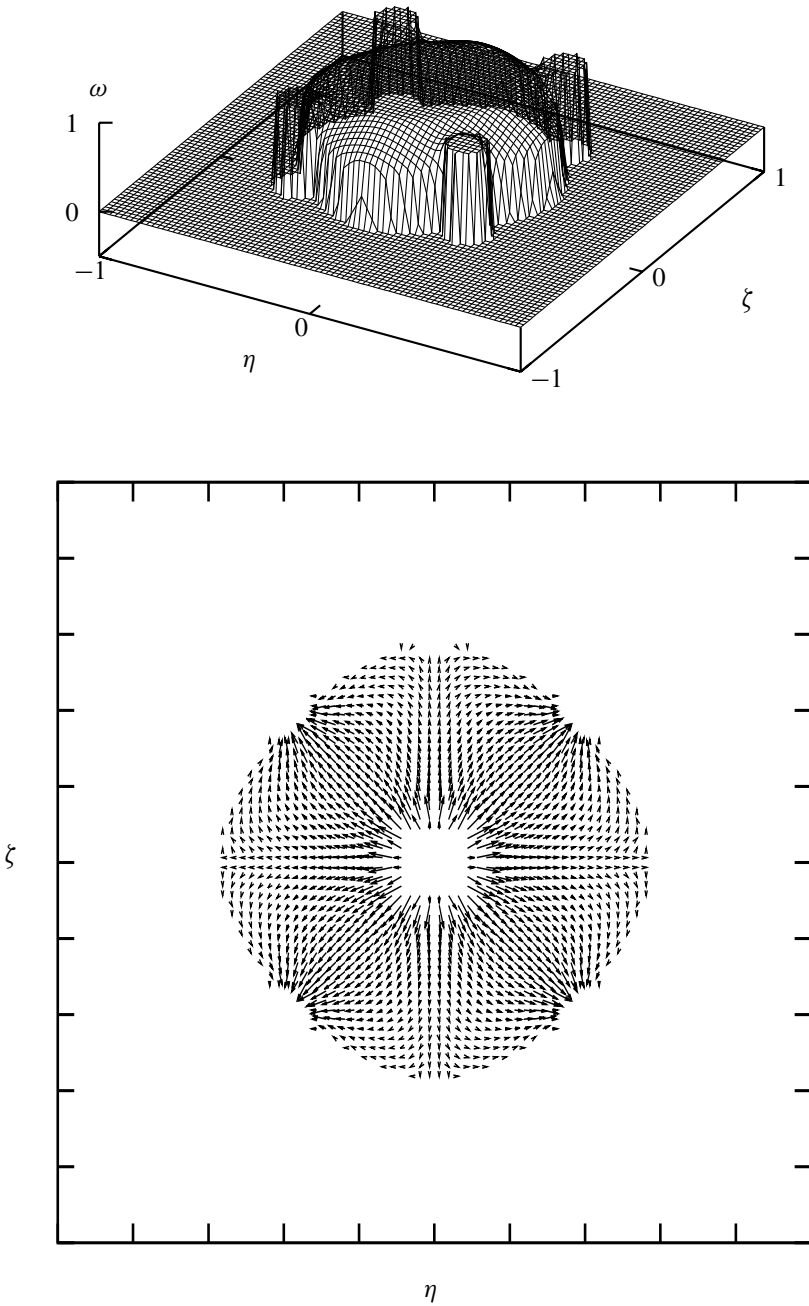


Figure 12. Damage (top) and fluid velocity field (bottom) at $\theta = 0.56$. The initial damage is the same as the one in [Figure 6](#).

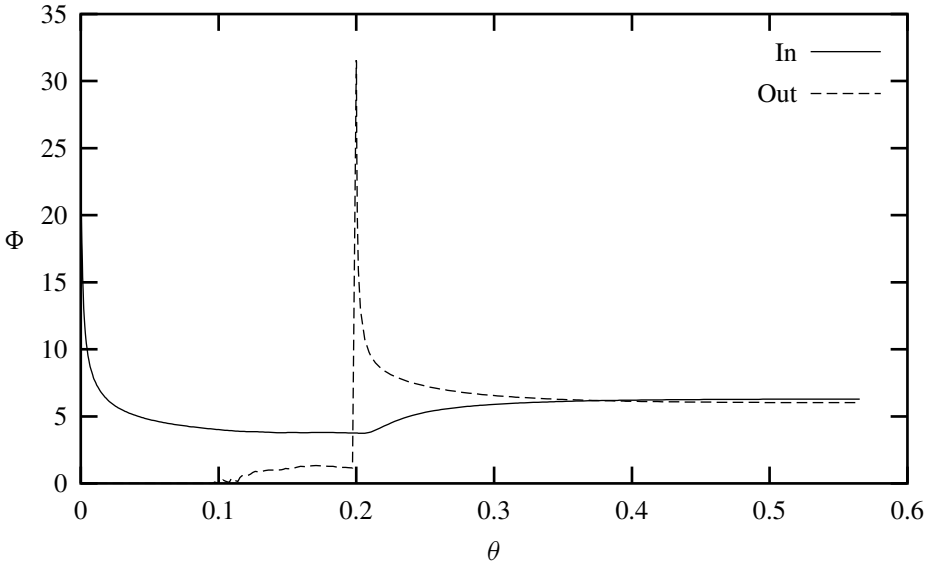


Figure 13. The total amount of fluid recovered per unit of time (Out), and the total amount of fluid injected per unit time (In), as functions of the nondimensional time θ . At $\theta \approx 0.1$ the damage front reaches the production wells. At $\theta = 0.2$ the production wells start working.

11. After a while the system seems to reach a stationary configuration, where both pressure and damage stop to evolve. As a consequence, all the fluid injected in the reservoir is caught by the production wells, as can be seen from Figures 12 and 13. So, from a mathematical point of view, the numerical simulations suggest that the 2D problem is well-posed, and that it has the structure of a free boundary problem, as was suggested in [2]. In this sense, the numerical experiments form a basis for further analytic studies. On the other hand, we are short of systematic quantitative studies of the microstructural changes of diatomites subjected to mechanical stress, and, in particular, the values of all the involved parameters are still unknown. Even merely a rough estimate of these parameters would make it possible to begin the simulation of real oilfields, a most important challenge for the future.

5. The one-dimensional formulation

In the following, we will deal with a flow to or from a drainage gallery described by the system (6). The numerical scheme adopted to solve this system is essentially the same as the one used for the 2D formulation. We begin our investigation by giving an overview of the behavior of the solutions. For this purpose we consider

on the interval $[0, 1]$ the system

$$\begin{cases} \partial_t \omega = \partial_x (\omega^\mu (p - I)_+^\beta \partial_x \omega) + A(1 - \omega)(p - I)_+^\gamma, \\ \partial_t p = \partial_x (\omega^\alpha \partial_x p), \end{cases} \quad (8)$$

where, without loss of generality, we have fixed $\Lambda = K = 1$. We choose initial data

$$\omega_0(x) = 0 \quad \text{for } x \in [0, 1]; \quad p_0(x) = 0.1 \quad \text{for } x \in [0, 1],$$

and boundary conditions

$$\partial_x \omega(0, t) = \partial_x \omega(1, t) = 0, \quad p(0, t) = 1.1 \quad \text{and} \quad p(1, t) = 0.1.$$

We observe that the physical condition of positiveness of $\partial_t \omega$ expressed in (6) has been removed, since it is never violated for these sets of initial and boundary conditions. We expect a damage-pressure front propagating from the left to the right.

We solved the problem numerically for several values of $\alpha, \beta, \gamma, \mu, I$. We selected some specific values that exhibit different types of behavior of the corresponding solutions and illustrate strong dependence on the parameters. This strong dependence will become even clearer when we investigate the traveling waves (section [Section 5.1](#)).

In [Figure 14](#) (top) we present the numerical approximations of the evolution of damage and pressure with $\alpha = 2, \beta = 0.5, \gamma = \mu = 1$ and $I = 0.8$. The simulation suggests that the damage is discontinuous across the free boundary. Moreover, the pressure seems to decrease linearly on the left side of the free boundary, towards a value which is reasonably close to the value $I \equiv 0.8$.

In the middle row of the same figure we selected instead $\alpha = 0.5, \beta = 2, \gamma = \mu = 1$ and $I = 0.6$, and the simulation suggests that ω goes down to zero smoothly near the free boundary.

Finally, in the bottom part of the figure we have chosen $\alpha = 2, \beta = 2, \gamma = \mu = 3$ and $I = 0.6$, and it seems that p jumps across the free boundary to a value greater than $I \equiv 0.6$, while ω seems to be continuous across the boundary.

Actually the numerical scheme is surprisingly stable near the free boundary, and preserves the sharpness of the boundary without smoothing it.

5.1. Traveling waves. A numerical investigation, the results of which were presented in the previous section, confirmed the conjecture that there exists a sharp front separating damaged ($\omega > 0$) and undamaged ($\omega = 0$) regions. Therefore, to investigate the *local structure* of such fronts (that is, the behavior of the flow characteristics close to the front), the studying of the traveling waves is appropriate. Naturally, the stretching of the horizontal coordinate is assumed, as it is always done when the structure of the fronts is considered (for example, the structure of

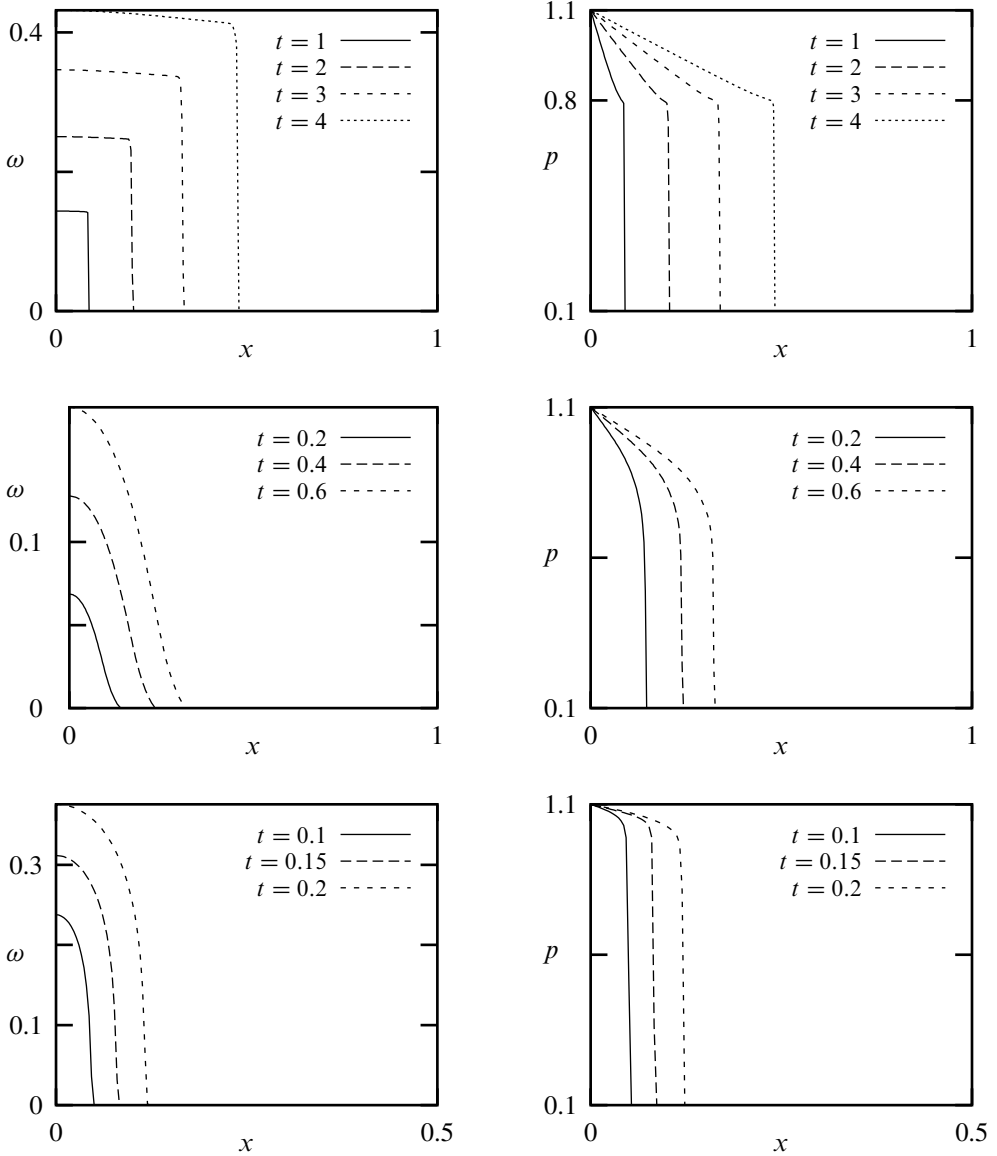


Figure 14. Numerical experiment. Left: damage; right: pressure.

Top: $\alpha = 2$, $\beta = 0.5$, $\gamma = \mu = 1$, $I = 0.8$; middle: $\alpha = 0.5$, $\beta = 2$, $\gamma = \mu = 1$, $I = 0.6$; bottom: $\alpha = 2$, $\beta = 2$, $\gamma = 1$, $\mu = 3$, $I = 0.6$.

the shock waves in gas dynamics). We focus our attention to the case of moving fronts. The rigorous mathematical investigation of the moving traveling waves can be found in [4]. At first, we refer to [5] and present some general mathematical

results concerning the existence of appropriate solutions for the system (8). In that paper, a solution (ω, p) is constructed in the case

$$\begin{aligned} \omega_0 > 0, \quad p_0 > 0 & \quad \text{in an interval } (a, b), \\ \omega_0 = p_0 = 0 & \quad \text{in } (-\infty, a) \text{ and } (b, \infty). \end{aligned}$$

It is proved in [5] that there exist two fronts, $x = a(t)$ and $x = b(t)$ (where $a(t)$ and $b(t)$ are continuous functions with $a(0) = a$, $b(0) = b$) which separate the damaged and undamaged rocks:

$$\begin{aligned} \omega(x, t) > 0, \quad p(x, t) > 0 & \quad \text{if } a(t) < x < b(t), \\ \omega(x, t) = p(x, t) = 0 & \quad \text{if } x < a(t) \text{ or } x > b(t). \end{aligned}$$

The product $\omega(p - I)_+$ is, generally speaking, continuous across the fronts at $t > 0$, which implies that at least one of the two functions ω and $(p - I)_+$ is continuous across the fronts at such times t . Moreover, if $p(x, 0) > I$ in the interval (a, b) , then $p(x, t) > I$ if $a(t) < x < b(t)$, $t > 0$. We emphasize that still very little is known mathematically about the general behavior of the solutions near the free boundary, and about the dependence of the solutions on the various parameters in the problem—this will be the problem of our further studies. In particular, it is important to know if ω or $(p - I)_+$ can be discontinuous across the free boundaries, as was suggested by the numerical simulations, and, if so, for which parameters.

Therefore we look for traveling waves of constant speed V , that is, for the solutions to the system (8) of the type $p = p(\xi)$, $\omega = \omega(\xi)$, $\xi = x - Vt$. For definiteness' sake, we assume that V is positive, and that both p and ω vanish when $\xi > 0$, and that $0 < \omega < 1$ and $p > I$ when $\xi_0 < \xi < 0$ for some negative ξ_0 . Under these assumptions, the system (8) leads to the system of ordinary differential equations

$$\begin{aligned} -V \frac{d\omega}{d\xi} &= \frac{d}{d\xi} (\omega^\mu (p - I)^\beta \frac{d\omega}{d\xi}) + A(1 - \omega)(p - I)^\gamma & \text{if } \xi_0 \leq \xi < 0, \\ -Vp &= \omega^\alpha \frac{dp}{d\xi} & \text{if } \xi_0 \leq \xi < 0, \end{aligned}$$

with the properties that $0 < \omega < 1$, $p > I$, $d\omega/d\xi < 0$ if $\xi_0 \leq \xi < 0$, and

$$\lim_{\xi \nearrow 0} \omega(p - I) = 0 = \omega^\mu (p - I)^\beta \frac{d\omega}{d\xi} + V\omega.$$

In [4] it has been shown that, for each choice of the values of the parameters and for each given value of the velocity $V > 0$, there exists a one-parameter family of solutions, and that the behavior of the traveling waves depends strongly on the values of the parameters. In particular, it has been shown that, for every $V > 0$, ω

can be discontinuous across the free boundary ($\xi = 0$) if and only if $0 < \beta < 1$ and $I > 0$. In such a case the traveling waves solutions behave near $\xi = 0$ as

$$\omega \approx \omega^* + \frac{V^{1-\beta}}{(1-\beta)I^\beta} (\omega^*)^{1+\alpha\beta-\mu} |\xi|^{1-\beta}, \quad p \approx I + V (\omega^*)^{-\alpha} I |\xi|,$$

where $\omega^* > 0$ is a free parameter. These analytic results are in agreement with the numerical results of [Figure 14\(a\)](#).

The question is more complicated if we consider for which parameter values there exist traveling waves for which $(p - I)_+$ is discontinuous across the interface. If $\mu \leq 1$ and $\alpha < \mu$, there again exists, for every velocity $V > 0$, a one-parameter family of traveling waves which, near the interface $\xi = 0$, behave as

$$\omega \approx B |\xi|^{1/\mu}, \quad p \approx p^* + C |\xi|^{1-\alpha/\mu}.$$

Here $p^* > I$ is the free parameter, and B and C are constants determined by V , p^* and by the parameters in the equations. But, if $\mu \geq 1$ and $\alpha < 1$, there exists as well, for every $V > 0$, a two-parameter family of solutions which behave as

$$\omega \approx B_1 |\xi|, \quad p \approx p^* + C_1 |\xi|^{1-\alpha}.$$

Here $p^* > I$ is one of the free parameters, and B_1 and C_1 are constants determined by V , p^* and by the parameters in the equations (but not by the second free parameter!).

The latter family has a remarkable property not satisfied by the former ones. Returning to the original variables of problem (6) we obtain new coefficients corresponding to B_1 and C_1 , and it turns out that they do not depend on the parameter Λ . As a matter of fact they coincide with the coefficients of the traveling wave solution of (6) if we put $\Lambda = 0$. Indeed, a straightforward calculation shows that if $\Lambda = 0$ and $0 < \alpha < 1$, then for any $p^* > I$ and $V > 0$ problem (6) has a traveling wave solution which, near the interface $x = Vt$ ($x < Vt$), behaves as

$$\omega \approx \frac{A(p^* - I)^\gamma}{V} |x - Vt|,$$

$$p \approx p^* \frac{V^{1+\alpha} p^*}{(1-\alpha)KA^\alpha (p^* - I)^{\alpha\gamma}} |x - Vt|^{1-\alpha}.$$

We refer to [\[4\]](#) for a detailed discussion on families of traveling wave solutions.

5.2. Optimization of oil recovery, a qualitative example of control problem.

In this section we consider an application of the 1D formulation (6) of the problem of fluid flow. Let the domain be the finite interval $0 \leq x \leq 1$. We are describing a flow to the “drainage galleries” placed in the section $x = 0$. We assume that such a drainage gallery can work both as an injection and a production one. This means

that it can work both at higher and lower pressure than the initial pressure of the oil reservoir p_i . It is feasible to suppose that $p_i \leq I$, since the value of I is the threshold pressure above which the microcracking starts to accumulate, and in the pristine state there are no cracks in the rocks. The system can be controlled by prescribing the pressure at $x = 0$, that is, in the gallery: we denote this value by $P(t)$. To start to extract oil, some amount of water is pumped through the wells (P is raised above I) in the diatomaceous stratum. Microcracks will appear inside the stratum and consequently the permeability of the rock will increase. After this initial process of water pumping, the pressure P is lowered below p_i in order to extract oil from the wells.

The problem of finding the best strategy to maximize the amount of extracted oil, as it was formulated, is ill-posed. In principle, a very long (in time) pulse, or a very high pulse for the function $P(t)$, would allow to damage regions very far from the wells. Moreover, there is no limitation on the amount of oil that can be taken out from this damaged zone, if we are able to decrease the pressure enough and wait for a long time.

However, the real conditions are far from this idealization, and there are several aspects that we have to take into account. First of all, a realistic assumption is that the device which controls the pressure in the wells, works only in a certain bounded range of pressure. Moreover, the whole process of oil extraction has several aspects to be taken into account by constructing a suitable “cost function” C . Therefore, we make the following assumptions:

- (1) There is a fixed cost k_1 per unit of time to maintain the gallery operating.
- (2) The cost per unit of time for injecting or extracting fluid is proportional to the power (work per unit time)

$$k_2 [-(P(t) - p_i) \Phi(t)]_+,$$

where p_i is the pressure of the wells at rest (we simplified the problem by considering the rest pressure in the wells equal to the initial pressure in the deposit), $\Phi(t)$ is the flux of liquid, and k_2 is a conversion factor.

- (3) The profit $F(t)$ is assumed to be proportional to the volume of extracted liquid $E(t)$:

$$F(t) = k_3 E(t).$$

Therefore, the total cost is $C(t) = k_1 t + k_2 \int_0^t [-(P(s) - p_i) \Phi(s)]_+ ds$. On the other hand,

$$\begin{aligned}
 F(t) &= -k_3 \left(\int_0^t K \omega^\alpha(0, t) \partial_x p(0, t) dt \right)_+ \\
 &= k_3 \left(\int_0^1 p(x, t) dx - \int_0^1 p(x, 0) dx \right)_+ \equiv (V(t))_+.
 \end{aligned}$$

Here $V(t)$ is the difference between the actual total volume and the initial total volume of fluid in the reservoir. Hence, the net profit is

$$G(t) = F(t) - C(t). \tag{9}$$

Our problem is to find the function $P(t)$ (with $0 \leq t \leq T$) that realizes the maximum of $G(T)$. Here T is some instant of time that can be fixed a priori, or can be included in the unknowns of the problem. We repeat that our formulation of the control problem is a schematic one, and is used here only for presenting and illustrating the basic idea.

We still need to specify the set of allowed control functions $P(t)$. We introduce two numerical examples where we make strong assumptions on the possible shape of $P(t)$.

Example 5.1. We assume that the device that regulates the pressure can only perform a single cycle consisting of the following steps:

- (1) *Injection and damaging.* Starting from the initial value of pressure p_i , the drainage gallery imposes a pulse of maximum amplitude p_{\max} ;
- (2) *Extraction.* After returning to the value p_i , the drainage gallery decreases the pressure linearly until a certain value p_{\min} is achieved, and keeps this value constant as long as the incoming flux ensures a profit;
- (3) *Back to the beginning.* The pressure increases linearly to its initial value p_i , so that the cycle is completed.

This cycle can be repeated as long as it is profitable. A cycle of $P(t)$ can be represented as follows (see [Figure 15](#)):

$$P(t) = \begin{cases} (p_{\max} - p_i) \sin\left(\pi \frac{t}{t_1}\right) + p_i & \text{if } 0 \leq t \leq t_1 \\ (-p_{\min} + p_i) \left(\frac{t_2 - t}{t_2 - t_1}\right)_+ + p_{\min} & \text{if } t_1 \leq t \leq t_3 \text{ and } t_2 < t_3 \\ (+p_{\min} - p_i) \left(\frac{t_4 - t}{t_4 - t_3}\right) + p_i & \text{if } t_3 \leq t \leq t_4. \end{cases} \tag{10}$$

The intervals t_1 , $t_2 - t_1$, and $t_4 - t_3$ are fixed a priori, but the interval $t_2 - t_3$ is not known a priori and is chosen by the program to optimize the profit in the cycle. In particular we keep the pressure at the drainage gallery equal to p_{\min} until the profit

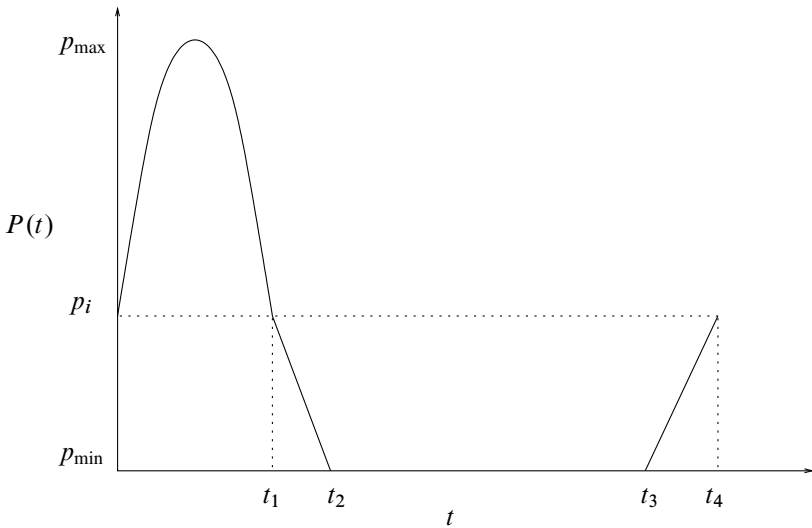


Figure 15. The cycle of the boundary pressure $P(t)$.

reaches a maximum ($G'(t_3) = 0$). Our choice is to optimize every single cycle, although, in case of several cycles, this is not necessarily the best global strategy.

For the numerical simulation we have chosen:

$$\begin{aligned}
 K = \Lambda = A = 1; & & I = 0.2; \\
 \alpha = \beta = 1; & & p_i = 0.1, \quad p_{\max} = 1, \quad \text{and} \quad p_{\min} = 0; \\
 \gamma = 5; & & t_1 = 0.2, \quad t_2 - t_1 = t_4 - t_3 = 0.04. \\
 \mu = 0
 \end{aligned}$$

To compute the cost function we have chosen:

$$k_1 = 0.01, \quad k_2 = 1, \quad k_3 = 20.$$

We have performed 5 cycles. As [Figure 16](#) clearly shows, the volume extracted at the end of the cycles increases with the number of cycles performed. However, we have to take into account the cost function $C(t)$, represented in [Figure 17](#). In fact, looking at the actual profit $G(t)$ in [Figure 18](#), we conclude that the best strategy consists in performing only two cycles.

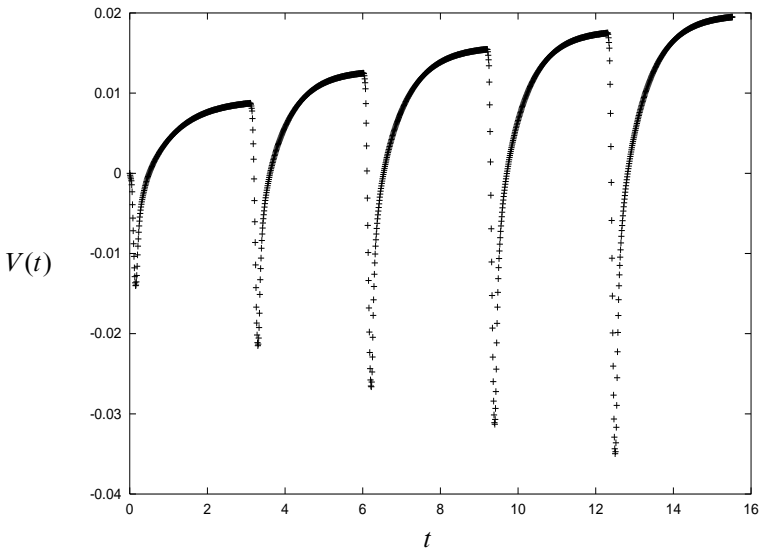


Figure 16. The volume function $V(t)$ is the difference between the volume extracted and injected. It increases with the number of pulses.

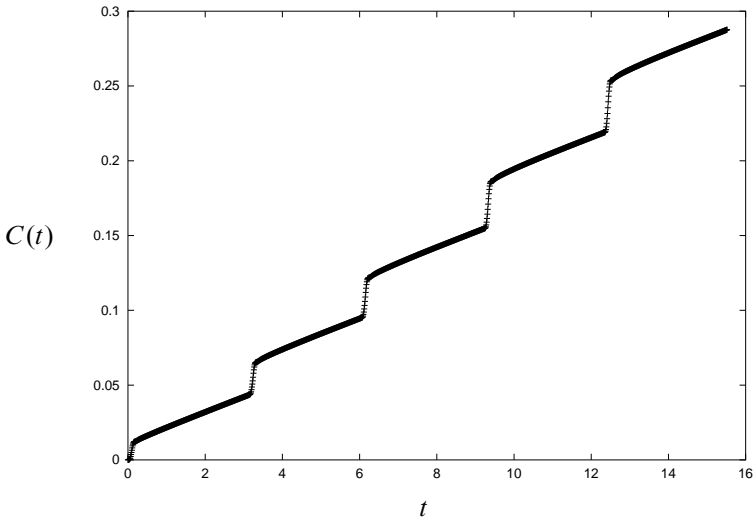


Figure 17. The cost function $C(t)$. The jumps correspond to fluid injections. During the injection, the main contribution is given by the integral term of the cost function. Between two jumps, instead, the cost increases almost linearly. This means that the main contribution is given by the time-linear term.

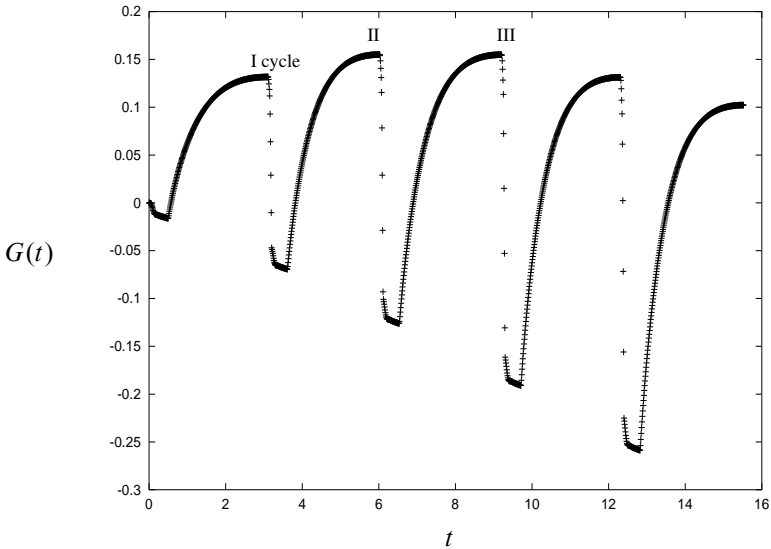


Figure 18. The profit function $G(t)$. The II pulse reaches the maximal profit, although the difference between the II and III pulses is very small (1.5511 versus 1.5496).

Example 5.2. We fix the total time T of the process and prescribe the form of the function $P(t)$ as in [Figure 19](#):

$$P(t) = \begin{cases} (p_{\max} - p_i) \sin\left(\pi \frac{t}{t_1}\right) + p_i & \text{if } 0 \leq t \leq t_1, \\ (-p_{\min} + p_i) \left(\frac{t_2 - t}{t_2 - t_1}\right) + p_{\min} & \text{if } t_1 \leq t \leq t_2, \\ 0 & \text{if } t_2 \leq t \leq T. \end{cases}$$

In this example t_1 is the unknown parameter which we use to optimize the profit function $G(T)$. For the sake of simplicity we prescribe the duration of the interval $t_2 - t_1$ to be equal to $T/10$. For the numerical simulation we have chosen

$$\begin{aligned} K = \Lambda = A = 1, & & I = 0.2, \\ \alpha = \beta = 1, & & p_i = 0.1, \quad p_{\max} = 1 \text{ and } p_{\min} = 0, \\ \gamma = 5, & & T = 3, \quad t_2 - t_1 = 0.3. \\ \mu = 0, & & \end{aligned}$$

We have evaluated numerically the profit function G for several values of the time t_1 . The results are shown in [Figure 20](#).

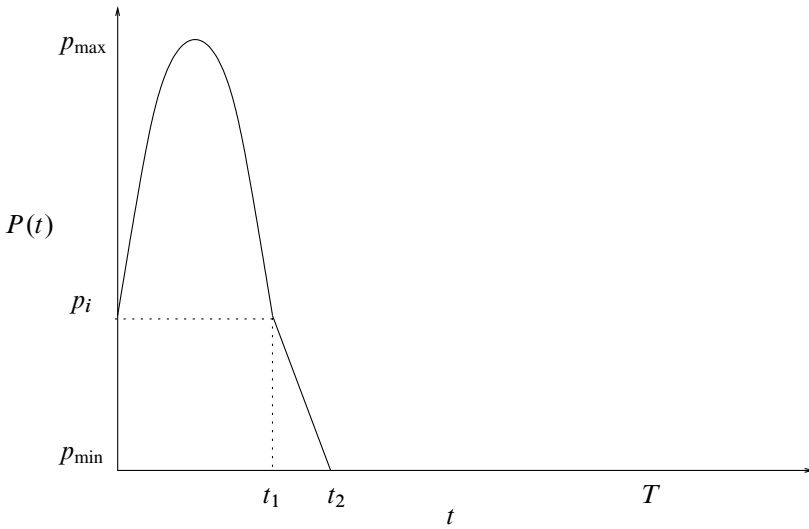


Figure 19. The boundary pressure $P(t)$.

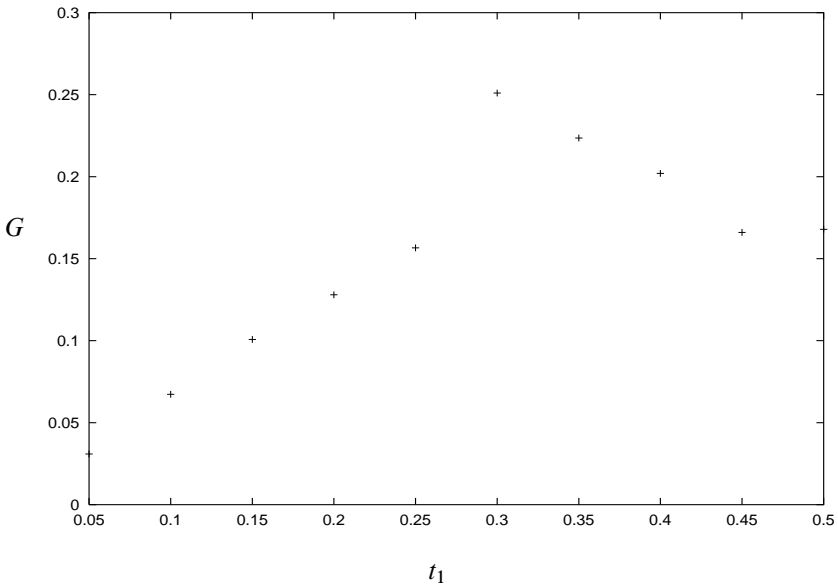


Figure 20. The profit function G as a function of the time t_1 .

Acknowledgments. This work was supported in part by the Director, Office of Science, Computational and Technology Research, U.S. Department of Energy, under Contract no. DE-AC03-76SF00098. Nitsch thanks the Lawrence Berkeley National Laboratory, where he carried most of his research, for its great hospitality.

All of us express our deep gratitude to Professor A. J. Chorin for his interest in this work, valuable advice and help. Our discussions with Professor T. W. Patzek, Dr. V. M. Prostokishin and Dr. D. B. Silin were very important for us in performing this work, and we express our deep gratitude to them.

References

- [1] G. I. Barenblatt, V. M. Entov, and R. V. M., *Theory of fluid flows through natural rocks*, Theory and applications of transport in porous media, vol. 3, Kluwer Academic Publishers, 1990.
- [2] G. I. Barenblatt, T. W. Patzek, V. M. Prostokishin, and D. B. Silin, *SPE75230: Oil deposit in diatomites: A new challenge for subterranean mechanics*, SPE/DOE Improved Oil Recovery Symposium, 2002.
- [3] J. Bear and Y. Bachmat, *Introduction to modeling of transport phenomena in porous media*, Kluwer Academic Publishers, 1991.
- [4] M. Bertsch and C. Nitsch, *Traveling wave solutions of a nonlinear degenerate parabolic system from petroleum engineering*, preprint, 2006.
- [5] M. Bertsch, R. Dal Passo, and C. Nitsch, *A system of degenerate parabolic nonlinear PDE's: a new free boundary problem*, *Interfaces Free Bound.* 7 (2005), no. 3, 255–276. [MR 2006f:35296](#) [Zbl 1079.35102](#)

Received September 28, 2005.

GRIGORY ISAAKOVICH BARENBLATT: gibar@math.berkeley.edu
Department of Mathematics, University of California, Berkeley CA 94720
and

*Lawrence Berkeley National Laboratory, 1 Cyclotron Road, Mail Stop 50A/1148,
Berkeley, CA 94720, United States*
<http://math.lbl.gov/barenblatt/barenblatt.html>

MICHIEL BERTSCH: m.bertsch@iac.cnr.it
*Istituto per le Applicazioni del Calcolo "Mauro Picone", Consiglio Nazionale delle Ricerche,
Viale del Policlinico, 137, I-00161 Roma, Italy*
and

*Dipartimento di Matematica, Università degli Studi di Roma "Tor Vergata", Via della Ricerca
Scientifica, I-00133 Roma, Italy*

CARLO NITSCH: carlo.nitsch@dma.unina.it
*Dipartimento di Matematica e Applicazioni "R. Caccioppoli", Università degli Studi di Napoli
"Federico II", Via Cintia, Monte S. Angelo, I-80126 Napoli, Italy*
<http://wpag.unina.it/c.nitsch/>